Cite as: A. Karton, *Chem. Phys.* 540, 111013 (2021).
https://doi.org/10.1016/j.chemphys.2020.111013

Can density functional theory 'Cope' with highly fluxional shapeshifting molecules?

Amir Karton*

[a]School of Molecular Sciences, The University of Western Australia, Perth, WA 6009, Australia.

A B S T R A C T

Shape-shifting molecules such as bullvalene undergo rapid structural reorganizations via degenerate Cope rearrangements. Here, we obtain accurate CCSD(T)/CBS barrier heights and reaction energies for a wide range of Cope rearrangements in substituted bullvalenes ($C_{10}H_9R$, R = NH_3, OH, CH_3, H, F, Cl, SH, and CN). We use this benchmark dataset to evaluate the performance of DFT and ab initio methods for the kinetics and thermodynamics of these reactions. The reaction barrier heights pose a significant challenge for DFT methods – the best methods attain root-mean-square deviations of 4.9 (BMK), 4.5 (PBE0), 4.2 (PW6B95), and 3.8 (B1B95) kJ mol^{-1}. Overall, only three DFT functionals (BMK, PW6B95, and MN12-SX) are able to surpass (or attain near) chemical accuracy for both barrier heights and reaction energies. In contrast, the double-hybrid DFT procedures ωB97X-2(LP), ωB97X-2(TQZ), PWPB95-D3, PBEQI-DH, and DSD-PBEB95-D3 give good-to-excellent performance.

Corresponding Author. Tel.: +61 8 6488 3139. E-mail: amir.karton@uwa.edu.au (A. Karton).

1. Introduction

Bullvalene ($C_{10}H_{10}$) and its derivatives are a fascinating class of fluxional carbon cages, which spontaneously undergo a series of degenerate Cope rearrangements.[1,2,3,4] These shapeshifting molecules have found several applications in functional materials, sensors, and biologically active compounds.[1,5,6,7,8,9,10,11,12,13,14,15] Since it can be difficult to investigate the potential energy surfaces (PESs) of highly fluxional molecules using experimental techniques, approximate theoretical procedures such as density functional theory (DFT)[10,13,15,16,17,18,19,20,21,22,23,24,25,26,27,28] and ab initio[16,17,20,22,23,28] methods often play a key role in these chemical explorations. In this context, it is worth mentioning the work of He and Bode which combined HPLC, NMR, and extensive DFT calculations to examine the potential energy surfaces and relative stabilities of substituted bullvalones.[10] It is therefore important to evaluate the performance of such approximate theoretical procedures in predicting the barrier heights and reaction energies of degenerate Cope rearrangements in bullvalene derivatives. Moreover, since DFT and ab initio methods are extensively used for modelling sigmatropic rearrangements in general, it is of interest to evaluate their performance for Cope rearrangements in bullvalene derivatives, which represent an intriguing example of sigmatropic shifts in strained hydrocarbon cages. A number of influential benchmark studies examined the performance of DFT methods for pericyclic reactions.[29,30,31,32,33] However, only a small subset of sigmatropic shifts were considered all of which involve simple hydrocarbons (e.g., 1,3-hexadiene, 1,5-hexadiene, and cyclopentadiene).

Here, we consider a wider set of 22 reaction barrier heights and 21 reaction energies in substituted bullvalene derivatives ($C_{10}H_9R$, R = NH_3, OH, CH_3, H, F, Cl, SH, and CN). We calculate the reaction energies and barrier heights of these reactions at the CCSD(T)/CBS level of theory by means of the W1-F12 composite procedure.[34,35] These benchmark values allow us to

assess the performance of a wide range of contemporary DFT and double-hybrid DFT methods across the rungs of Jacob's Ladder,[36] as well as MP2-based and composite ab initio methods.

2. Computational Methods

We use the high-level W1-F12 composite procedure for obtaining reaction energies and barrier heights at the CCSD(T)/CBS level (i.e., coupled cluster with single, double, and quasiperturbative triple excitations close to the complete basis set limit). The computational protocol of W1-F12 theory has been specified and rationalized elsewhere,[34] and W1-F12 theory has been found to give thermochemical and kinetic properties with sub-kcal-per-mole accuracy for hydrocarbons.[34,35,37,38,39,40] In this context, it is worth mentioning that the largest systems considered in the present work consist of 12 non-hydrogen atoms ($C_{11}H_9N$). Each of the W1-F12 calculations for these systems ran for about 5 days on 16 cores of a dual Intel Xeon machine (E5-2683-v3 and 2.0 GHz) with 256 GB of RAM. In contrast, a DFT single point energy calculation for the same system requires less than an hour to complete on 4 cores and 16 GB of RAM.

The DFT exchange-correlation (XC) functionals considered in the present study (ordered by their rung on Jacob's Ladder)[36] are given in Table 1. Empirical D3 dispersion corrections[41,42,43] are included in some cases using the finite Becke–Johnson[44] and zero-damping potentials (denoted by D3BJ and D3, respectively).

Table 1. DFT exchange-correlation functionals and standard/composite ab initio methods considered in the present work.

Type[a]	Functionals
GGA	BLYP,[45,46] B97-D,[47] HCTH407,[48] PBE,[49] BP86,[45,50] BPW91,[46,51] SOGGA11,[52] N12[53]
MGGA	M06-L,[54] TPSS,[55] τ-HCTH,[56] VSXC,[57] BB95,[58] M11-L,[59] MN12-L,[60] MN15-L[61]
HGGA	BH&HLYP,[62] B3LYP,[45,63,64] B3P86,[63,50] B3PW91,[63,51] PBE0,[65] B97-1,[66] B98,[67] X3LYP,[68] SOGGA11-X,[69] APF,[70] mPW1PW91,[71,51] mPW1PBE,[71,49] mPW1LYP,[45,71] CAM-B3LYP,[b,72] ωB97X-V,[b,73] N12-SX[b,74]
HMGGA	M05,[75] M05-2X,[76] M06,[77] M06-2X,[77] M06-HF,[77] M08-HX,[78] MN15,[61] BMK,[79] B1B95,[45,58] TPSSh,[80] τ-HCTHh,[56] PW6B95,[81] MN12-SX,[b,74] M11,[b,82] ωB97M-V[b,83]
DH	B2-PLYP,[84] B2GP-PLYP,[85] B2K-PLYP,[86] DSD-BLYP,[87] DSD-PBEP86-D3BJ,[88,89] DSD-PBEB95,[88] PBE0-DH,[90] XYG3,[91] PWPB95,[92] PBEQI-DH,[93] ωB97X-2(LP),[94] ωB97X-2(TQZ),[94] ωB97M-2[95]
MP	MP2, S2-MP2,[96] SCS-MP2,[97] SCS-MP2(vdW),[98]SOS-MP2[99]
Ab Initio	G4,[100] G4(MP2),[101] G4(MP2)-6X,[102] CBS-QB3[103]

[a]GGA = generalized gradient approximation, MGGA = meta-GGA, HGGA = hybrid-GGA, HMGGA = hybrid-meta-GGA, DH = double hybrid, MP = Møller–Plesset perturbation theory, Ab Initio = composite ab initio methods. [b]Range separated XC functional.

All the standard DFT calculations were carried out in conjunction with the Def2-TZVPP basis set, whilst the DHDFT and MP2 calculations, due to their slower basis set convergence,[104] were carried out in conjunction with the Def2-QZVPP basis set.[105] All the CCSD(T) calculations involved in W1-F12 theory were calculated using Molpro 2016,[106,107] whilst all the other calculations (DFT, DHDFT, MP2, and lower-level composite procedures) were performed using the Gaussian 16 and Q-Chem 5.2 program suites.[108,109]

3. Results and Discussion

3.1. Overview of the reactions and benchmark CCSDT(Q)/CBS reaction barrier heights in the CopeBH database. The Cope database is comprised of reaction energies and barrier heights in substituted bullvalenes ($C_{10}H_9R$, R = NH_3, OH, CH_3, H, F, Cl, SH, and CN). For each R group we consider three transition structures for the Cope rearrangements which are schematically illustrated in Figure 1 (**TS**$_{1\text{-}2}$, **TS**$_{2\text{-}3}$, and **TS**$_{3\text{-}4}$). Note that for R = H there is only one unique TS for all the possible Cope rearrangements. The resulting 22 reaction barrier heights are referred to as the CopeBH subset. We also evaluate the performance approximate DFT and ab initio procedures for the relative energies of the reaction intermediates in the Cope database (structures **2**, **3**, and **4**, Figure 1). Note that there the reaction energy for R = H is nil. The resulting 21 reaction energies are referred to as the CopeRE subset. All reaction energies and barrier heights are calculated relative to structure **1** in Figure 1. We calculate the reaction energies and barrier heights at the CCSD(T)/CBS level of theory by means of the W1-F12 composite procedure.[34] It has been recently shown that CCSD(T)/CBS reaction barrier heights benefit from an effective error cancellation between the higher-order triples, T–(T), which tend to increase the barrier heights, and the quasiperturbative quadruples, (Q), which tend to reduce the barrier heights.[37] Table 2 lists the CCSD(T)/CBS reaction energies (ΔE_r) and barrier heights ($\Delta E^{\ddagger}$) for the reactions in the Cope database.

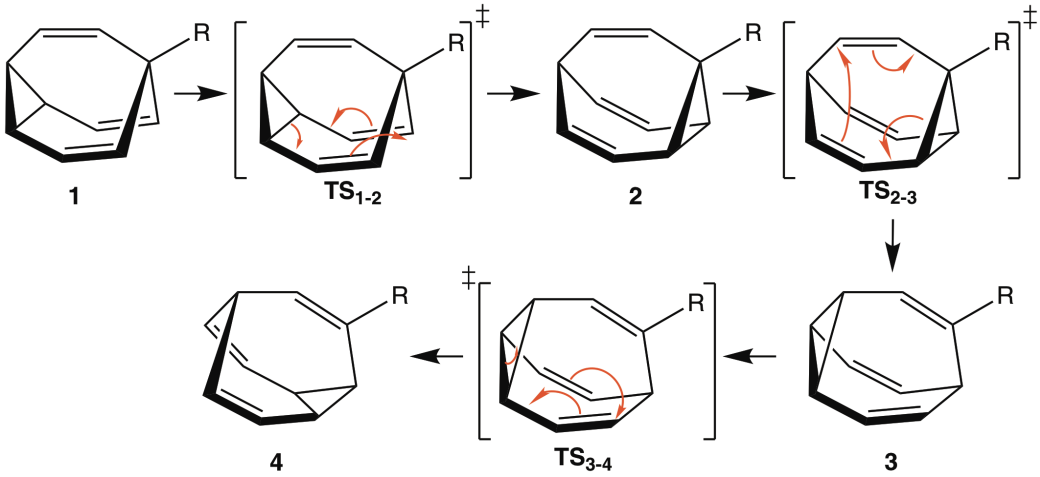

Figure 1. Schematic representation of the unimolecular rearrangements in the Cope database (R = NH_3, OH, CH_3, H, F, Cl, SH, and CN).

Table 2. CCSD(T)/CBS reaction barrier heights ($\Delta E^{\ddagger}$) and energies (ΔE_r) for the reactions in the Cope database obtained by means of W1-F12 theory (in kJ mol^{-1}).[a]

	$\Delta E^{\ddagger b}$		$\Delta E_r{}^c$	
R	**Structure**		**Structure**	
H	**TS**	63.24	N/A	N/A
NH_3	**TS1-2**	58.70	**2**	–1.91
NH_3	**TS2-3**	48.18	**3**	–15.94
NH_3	**TS3-4**	45.18	**4**	–14.04
OH	**TS1-2**	66.25	**2**	5.71
OH	**TS2-3**	62.89	**3**	–3.39
OH	**TS3-4**	58.44	**4**	–11.95
CH_3	**TS1-2**	60.74	**2**	–0.03
CH_3	**TS2-3**	64.31	**3**	–3.63
CH_3	**TS3-4**	58.60	**4**	–2.80
F	**TS1-2**	65.14	**2**	14.96
F	**TS2-3**	79.22	**3**	7.60
F	**TS3-4**	69.38	**4**	6.23
SH	**TS1-2**	63.81	**2**	–5.59
SH	**TS2-3**	50.79	**3**	–12.97
SH	**TS3-4**	50.72	**4**	–11.21
Cl	**TS1-2**	63.79	**2**	4.40
Cl	**TS2-3**	64.36	**3**	–4.93
Cl	**TS3-4**	58.44	**4**	–4.32
CN	**TS1-2**	64.31	**2**	–9.71
CN	**TS2-3**	41.18	**3**	–21.36
CN	**TS3-4**	45.93	**4**	–17.47

[a]All values are relative to structure **1**. [b]All-electron, nonrelativistic, vibrationless CCSD(T)/CBS reaction barrier heights. [c]All-electron, nonrelativistic, vibrationless CCSD(T)/CBS reaction energies.

The nonrelativistic, all-electron, vibrationless CCSD(T)/CBS reaction barrier heights in the Cope database spread over a wide energetic range from 41.2 (**TS$_{2\text{-}3}$**, R = CN) to 79.2 (**TS$_{2\text{-}3}$**, R = F) kJ mol^{-1}. It is of interest to examine the substituent effect on the reaction barrier height for each of the TSs (**TS$_{1\text{-}2}$**, **TS$_{2\text{-}3}$**, and **TS$_{3\text{-}4}$**). Figure S1 of the Supporting Information gives a plot of the reaction barrier height as a function of the σ_p Hammett constants for the various substituents. As can be seen there is no apparent correlation between the electron withdrawing/donating capability of the substituents and the reaction barrier heights. However, it is clear that the substituent effect on the stability of **TS$_{2\text{-}3}$** and **TS$_{3\text{-}4}$**, in which the substituent is connected to one of the sp^2 carbons of the hydrocarbon bridge, is much larger than that on **TS$_{1\text{-}2}$**, in which the substituent is connected to one of the sp^3 bridgehead carbons (Figures 1 and S1). For example, the difference between the W1-F12 reaction barrier heights for the various substituents spreads over a relatively narrow range of 7.6 kJ mol^{-1} for **TS$_{1\text{-}2}$**, however for **TS$_{2\text{-}3}$** and **TS$_{3\text{-}4}$** the reaction barriers are affected by as much as 38.0 and 24.2 kJ mol^{-1}, respectively by the substituents.

Based on the W1-F12 reaction barrier heights, we predict that the most rapid rearrangements would occur for R = NH_3 with a rate-determining step (RDS) of 58.7 kJ mol^{-1} obtained for **TS$_{1\text{-}2}$**. The slowest rearrangements are expected to occur for R = F with an RDS of 79.2 kJ mol^{-1} obtained for **TS$_{2\text{-}3}$**. For most of the substituents (NH_3, OH, H, SH, and CN) **TS$_{1\text{-}2}$** is the RDS for the series of Cope rearrangements, whilst for CH_3, F, and Cl **TS$_{2\text{-}3}$** is the RDS. Thus, there is no apparent correlation between the electron withdrawing/donating capability of the substituent and the RDS.

The reaction energies in the Cope database also spread over a relatively large energetic range from –21.36 (**3**, R = CN) to 14.96 (**2**, R = F) kJ mol^{-1}. Most of the reaction energies are exothermic, however, in some cases they can be endothermic (most notably for R = F).

Table 3 lists the component breakdown of the all-electron, nonrelativistic W1-F12 reaction barrier heights in the Cope database. The reaction barrier heights are severely

overestimated at the SCF level by amounts ranging from 34.9 (**TS**$_{2\text{-}3}$, R = NH_3) to 49.4 (**TS**$_{3\text{-}4}$, R = F) kJ mol^{-1}. The valence CCSD correlation component systematically reduces the reaction barrier heights by amounts ranging from 20.0 (**TS**$_{2\text{-}3}$, R = NH_3) to 30.2 (**TS**$_{3\text{-}4}$, R = F) kJ mol^{-1}. The (T) correlation contribution is still chemically very significant and systematically reduces the reaction barrier heights by amounts ranging between 15.3 (**TS**$_{3\text{-}4}$, R = F) and 20.6 (**TS**$_{2\text{-}3}$, R = NH_3) kJ mol^{-1}. These results are consistent with results obtained for a wide and diverse set of pericyclic reaction barrier heights for which both the CCSD and (T) correlation components systematically and significantly reduce the reaction barrier heights.[29,37] The CCSD(T) core-valence corrections to the reaction barrier heights are fairly modest and do not significantly exceed the 1 kJ mol^{-1} mark.

Table 3. Component breakdown of the all-electron, nonrelativistic CCSD(T)/CBS reaction barrier heights ($\Delta E^{\ddagger}$) and energies (ΔE_r) for the reactions in the Cope database obtained by means of W1-F12 theory (in kJ mol^{-1}, for each substituent energies are given relative to reactant **1**).

		$\Delta E^{\ddagger b}$					ΔE_r [c]			
R	**Structure**	**SCF**	**CCSD**	**(T)**	**CV**[a]	**Structure**	**SCF**	**CCSD**	**(T)**	**CV**[a]
H	**TS**	108.1	–26.8	–19.5	1.3	N/A	N/A	N/A	N/A	N/A
NH_3	**TS**$_{1\text{-}2}$	102.1	–25.7	–19.1	1.3	**2**	–3.6	1.5	0.3	–0.2
NH_3	**TS**$_{2\text{-}3}$	83.0	–20.0	–15.3	0.5	**3**	–17.7	2.3	0.1	–0.7
NH_3	**TS**$_{3\text{-}4}$	87.4	–23.8	–19.0	0.7	**4**	–16.3	2.6	0.3	–0.6
OH	**TS**$_{1\text{-}2}$	110.3	–26.3	–19.1	1.4	**2**	5.4	0.3	0.1	–0.1
OH	**TS**$_{2\text{-}3}$	105.2	–25.6	–17.6	0.9	**3**	–0.3	–1.9	–0.8	–0.4
OH	**TS**$_{3\text{-}4}$	105.3	–28.0	–19.8	0.9	**4**	–11.2	–0.1	–0.4	–0.4
CH_3	**TS**$_{1\text{-}2}$	105.0	–26.2	–19.4	1.4	**2**	–2.1	1.7	0.4	–0.1
CH_3	**TS**$_{2\text{-}3}$	107.1	–24.8	–19.1	1.2	**3**	–8.5	4.1	0.9	–0.2
CH_3	**TS**$_{3\text{-}4}$	98.0	–22.1	–18.5	1.2	**4**	–8.0	4.4	0.9	–0.1
F	**TS**$_{1\text{-}2}$	109.0	–26.3	–18.9	1.3	**2**	15.8	–0.8	–0.1	–0.1
F	**TS**$_{2\text{-}3}$	127.8	–30.0	–19.7	1.1	**3**	12.0	–3.4	–0.7	–0.3
F	**TS**$_{3\text{-}4}$	118.8	–30.2	–20.2	1.1	**4**	10.5	–3.2	–0.8	–0.2
SH	**TS**$_{1\text{-}2}$	108.6	–26.5	–19.6	1.4	**2**	–9.6	3.3	0.7	0.0
SH	**TS**$_{2\text{-}3}$	89.9	–22.3	–18.0	1.2	**3**	–17.4	3.9	0.6	–0.1
SH	**TS**$_{3\text{-}4}$	90.9	–22.6	–18.8	1.2	**4**	–16.4	4.6	0.8	–0.1
Cl	**TS**$_{1\text{-}2}$	109.0	–26.9	–19.7	1.3	**2**	2.2	1.6	0.6	–0.1
Cl	**TS**$_{2\text{-}3}$	108.8	–26.8	–18.8	1.1	**3**	–5.3	0.3	0.3	–0.2
Cl	**TS**$_{3\text{-}4}$	103.1	–26.4	–19.3	1.1	**4**	–4.9	0.6	0.2	–0.2
CN	**TS**$_{1\text{-}2}$	110.0	–27.3	–19.8	1.3	**2**	–11.6	2.3	–0.4	0.0
CN	**TS**$_{2\text{-}3}$	79.3	–20.2	–19.1	1.2	**3**	–22.2	2.3	–1.4	–0.2
CN	**TS**$_{3\text{-}4}$	89.9	–24.5	–20.6	1.2	**4**	–19.8	3.3	–0.8	–0.1

[a]Core-valence correction.

Table 3 lists the component breakdown of the W1-F12 CCSD(T)/CBS reaction energies in the Cope database. Inspection of these results reveals chemically significant contributions from the CCSD component in many cases. It is worthwhile highlighting a few cases here. At the SCF/CBS level, the reaction energy for the **1** → **3** rearrangement (R = OH) is –0.3 kJ mol^{-1}. The CCSD/CBS correlation component reduces this reaction energy by 1.9 kJ mol^{-1} and the (T) component further reduces it by 0.8 kJ mol^{-1}. Another interesting example is the **1** → **2** rearrangement (R = CH_3). The reaction energy at the SCF/CBS level is –2.1 kJ mol^{-1}. The CCSD and (T) correlation contributions increase this reaction energy by 1.7 and 0.4 kJ mol^{-1},

respectively. Thus, perfectly cancelling the SCF component and resulting in an overall CCSD(T)/CBS reaction energy of 0.0 kJ mol^{-1}. Similar to the reaction barrier heights, core-valence contributions play a fairly minor role in the reaction energies.

3.2 Performance of DFT and ab initio procedures for the reaction barrier heights in the CopeBH database. Table S1 of the Supporting Information gives the root mean square deviations (RMSDs), mean absolute deviations (MADs), and mean signed deviations (MSDs) for the DFT exchange-correlation functionals considered in the present work, whilst the RMSDs are depicted in Figure 2. Figure 2a gives the RMSDs for the GGA (rung 2) and MGGA (rung 3) functionals in order of decreasing RMSDs. Inspection of these results shows that the GGAs are mostly concentrated on the left side of the plot with large RMSDs of over 20 kJ mol^{-1}. The best performing GGA functional is HCTH407 with an RMSD of 14.2 kJ mol^{-1}. The MGGA methods are mostly concentrated on the right side of the plot with RMSDs below 20 kJ mol^{-1}. The one functional that attains an RMSD close to the chemical accuracy threshold is M06-L with an RMSD of 5.3 kJ mol^{-1}.

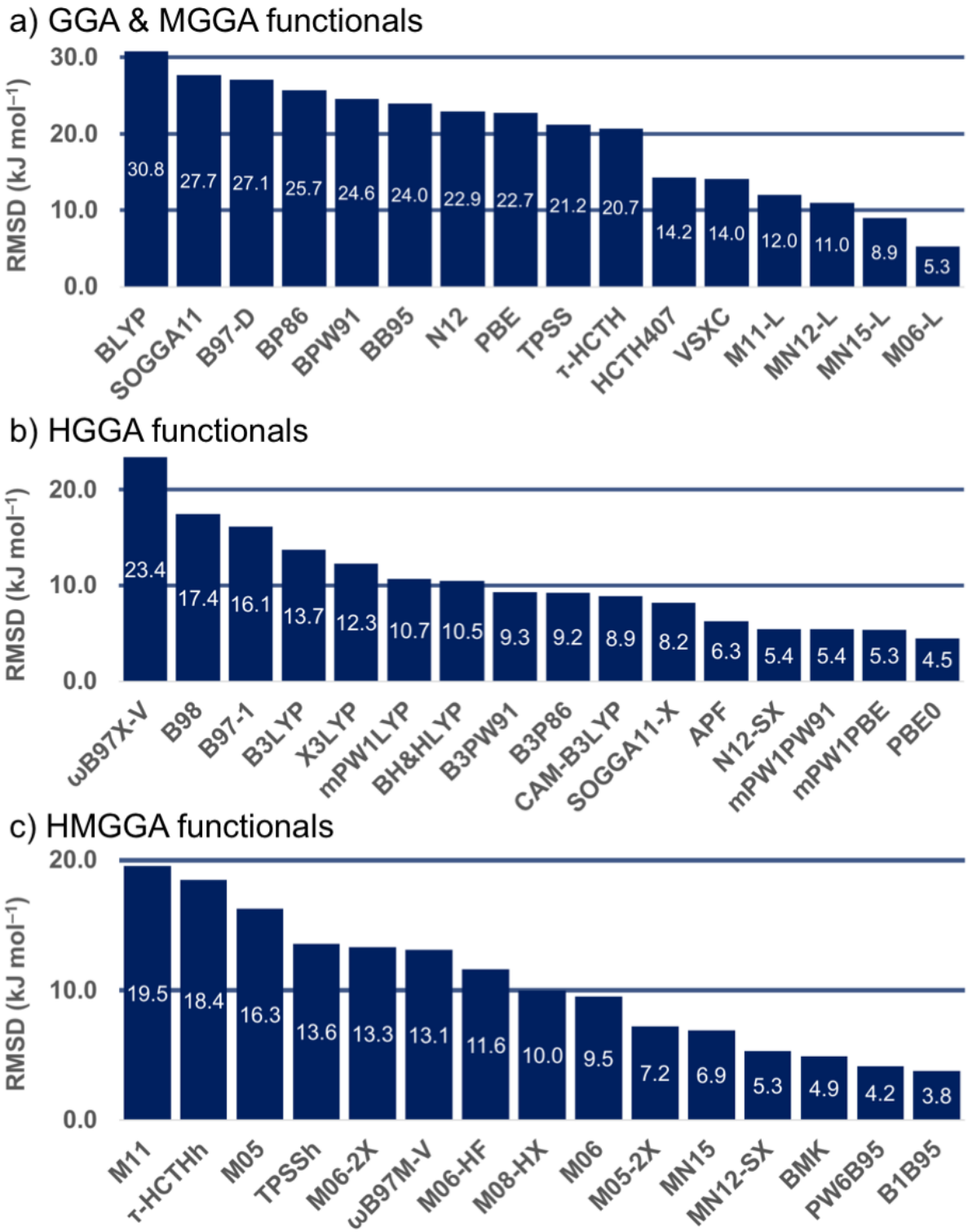

Figure 2. Root-mean-square deviations for (a) GGA and MGGA, (b) HGGA, and (c) HMGGA functionals over the barrier heights in the CopeBH database (in kJ mol^{-1}) (note that GGAs and MGGAs belong to different rungs of Jacob's Ladder but are grouped to save space).

Figure 2b gives the RMSDs for the global and range-separated HGGA functionals. With the exception of PBE0 which attain an RMSD of 4.5 kJ mol^{-1}, none of the HGGA functionals show better performance than the best MGGA functional M06-L. The global hybrids mPW1PW91 and mPW1PBE as well as the range-separated N12-SX attain similar performance to M06-L with RMSDs of 5.3–5.4 kJ mol^{-1}. Interestingly, PBE0, mPW1PW91, mPW1PBE, and N12-SX (in the short range) all involve 25% of exact Hartee–Fock (HF) exchange. It should be noted that mPW1LYP, which attains a much higher RMSD of 10.7 kJ mol^{-1} also involves 25% of exact HF exchange. Nevertheless, it seems like the LYP correlation functional gives poor performance across the board. For example, BLYP is the worst performing GGA functional (RMSD = 30.8 kJ mol^{-1}) and B3LYP, X3LYP, mPW1LYP, and BH&HLYP all attain RMSDs > 10 kJ mol^{-1}, regardless of the percentage of exact HF exchange involved in the XC functional.

Inspection of Figure 2 shows that the HMGGA functionals still struggle with the reaction barrier heights in the CopeBH database. The only three functionals that show better performance than the MGGA functional M06-L are (RMSDs given in parentheses): BMK (4.9), PW6B95 (4.2), and B1B95 (3.8 kJ mol^{-1}). The excellent performance of PW6B95 and B1B95 is in sharp contrast to the very poor performance of the MGGA functional BB95 (RMSD = 24.0 kJ mol^{-1}) which also uses the Becke95 correlation functional.[58] The range-separated HMGGA MN12-SX (RMSD = 5.3 kJ mol^{-1}) shows very similar performance its HGGA counterpart N12-SX. The other HMGGA functionals from the Minnesota family show poorer performance with RMSDs between 6.9 (MN15) and 19.5 (M11) kJ mol^{-1}.

Table S1 of the Supporting Information gives the MAD/RMSD ratios for the considered DFT functionals. Inspection of these ratios reveals that for about 60% of the considered DFT functionals it is ≥ 0.95 indicating a large systematic error across the dataset, whilst for about 20% of the DFT functionals this ratio approaches the $\sqrt{2/\pi} \approx 4/5$ limit indicating a small systematic error for a purely Gaussian error distribution.[110,111] Thus, it is instructive to examine more closely

the effect of the various substituents (NH_3, OH, CH_3, H, F, Cl, SH, and CN) on the performance of DFT functionals. Table S2 of the Supporting Information gives the deviations from W1-F12 theory for all the substituents and DFT functionals. Upon inspection of the results in Table S2 a few interesting trends emerge. The deviations for **TS**$_{1\text{-}2}$, in which the substituent is connected to one of the two sp^3 bridgehead carbons (Figure 1) are little affected by the electron donating/withdrawing strength of the substituent. For example, the deviations from W1-F12 theory across the substituents are fairly constant, i.e., they normally vary by about 1.5 kJ mol^{-1} (Table S2). On the other hand, for **TS**$_{2\text{-}3}$ and **TS**$_{3\text{-}4}$, in which the R substituent is connected to an sp^2 carbon of the hydrocarbon bridge (Figure 1), the substituents have a significantly more pronounced effect on the deviations from W1-F12 theory. In these cases, the effect of the substituent on the deviation from W1-F12 theory are over ~6 kJ mol^{-1} on average and can exceed 10 kJ mol^{-1}. To illustrate these points let us look at the spread of errors for the various substituents for two popular DFT functionals – BLYP and B3LYP. The error range, ΔErr, is defined as the difference between the maximum and minimum errors over the seven substituents. For BLYP, we obtain ΔErr = 1.5 (**TS**$_{1\text{-}2}$), 7.2 (**TS**$_{2\text{-}3}$), and 7.9 (**TS**$_{3\text{-}4}$) kJ mol^{-1}, and similar error ranges are obtained for B3LYP, namely ΔErr = 1.0 (**TS**$_{1\text{-}2}$), 6.3 (**TS**$_{2\text{-}3}$), and 6.8 (**TS**$_{3\text{-}4}$) kJ mol^{-1}. To further illustrate this point let us look at two additional DFT methods from a different family – M06-L and M06. For M06-L, we obtain ΔErr = 1.4 (**TS**$_{1\text{-}2}$), 6.8 (**TS**$_{2\text{-}3}$), and 6.2 (**TS**$_{3\text{-}4}$) kJ mol^{-1}, whilst for M06 ΔErr = 1.2 (**TS**$_{1\text{-}2}$), 7.4 (**TS**$_{2\text{-}3}$), and 5.4 (**TS**$_{3\text{-}4}$) kJ mol^{-1}. Similar trends are observed for the other functionals (Table S2). Inspection of the results in Table S2 also reveals that, with few exceptions, the largest errors for **TS**$_{2\text{-}3}$ and **TS**$_{3\text{-}4}$ are obtained for the strong electron-donating and -accepting substituents NH_3 and CN.

Inspection of the MADs and MSDs in Table S1 reveals that, as expected,[112113,114] most conventional DFT functionals tend to systematically underestimate the reaction barrier heights, as evident from MSD ≈ –1×MAD. The main exceptions include functionals with large percentages

of exact HF exchange (e.g., BH&HLYP, SOGGA11-X, M05-2X, M06-2X, M06-HF, M08-HX, and MN15) and range-separated functionals (e.g., CAM-B3LYP, M11, ωB97M-V, and ωB97X-V).

Figure 3 depicts the RMSDs for the MP2-based and double-hybrid DFT methods, both of which have similar computational costs. Remarkably, the MP2-based methods are amongst the best and worst methods with RMSDs of 25.8 (MP2), 21.3 (S2-MP2), 15.3 (SCS-MP2(vdW)), 7.5 (SCS-MP2), and 1.9 (SOS-MP2) kJ mol^{-1}. Inspection of the scaling factor for the same-spin component (C_{SS}) of the MP2 correlation energy reveals that there is a linear correlation (R^2 = 0.978) between the RMSD and the magnitude of the scaling factor. This linear correlation is depicted in Figure 4. This result is consistent with the improved performance of SCS-MP2 (C_{SS} = 1/3) over MP2 for the 26 barrier heights of pericyclic reactions in the BHPERI database.[29]

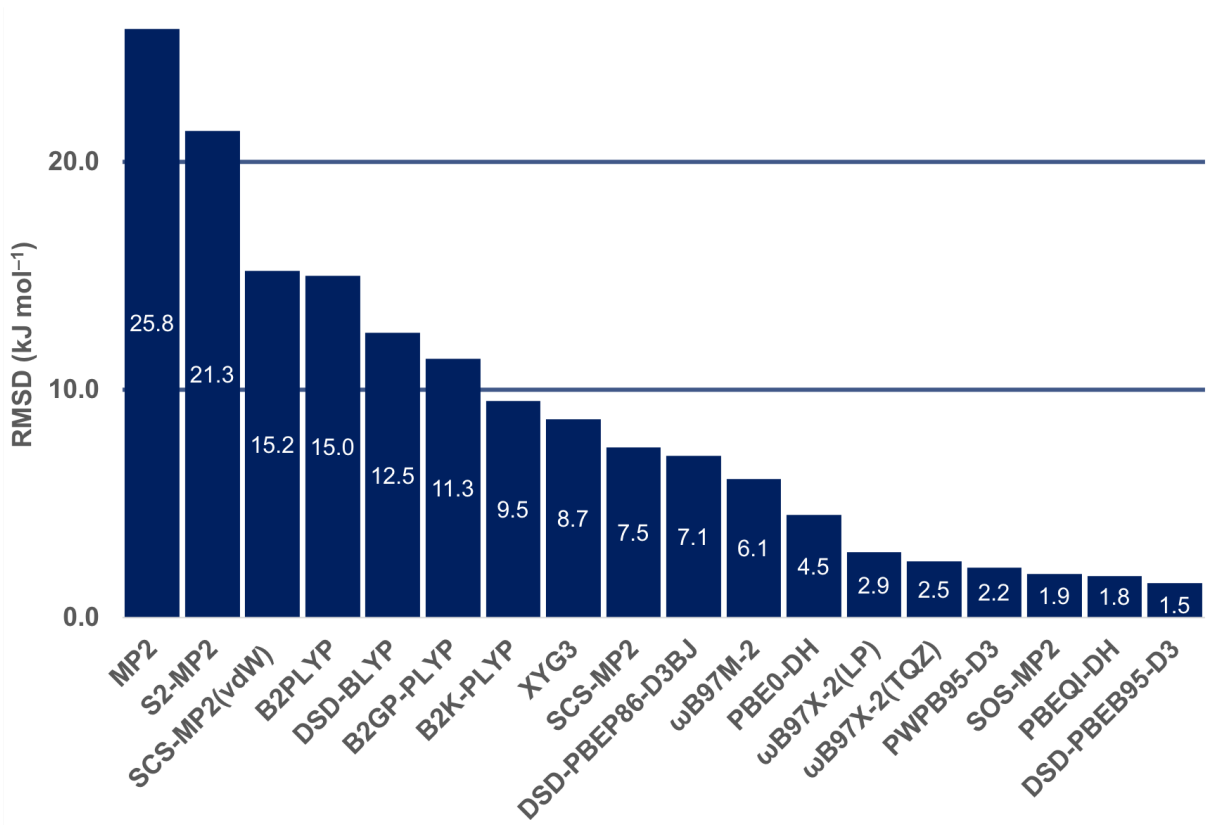

Figure 3. Root-mean-square deviations for DHDFT and standard/composite ab initio methods over the barrier heights in the CopeBH database (in kJ mol^{-1}).

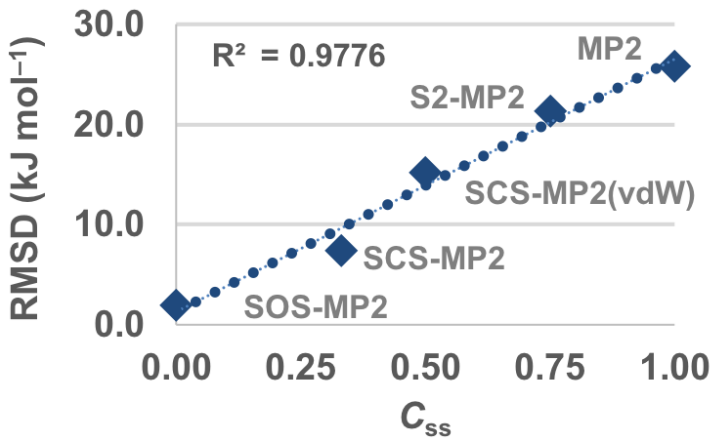

Figure 4. Near-linear correlation between the same-spin component of the MP2 correlation energy (C_{ss}) and the RMSDs for the MP2-based methods over the barrier heights in the CopeBH database (in kJ mol^{-1}).

Figure 3 shows that the reaction barrier heights in the Cope database pose a challenging problem for DHDFT methods. The older generation methods, which do not involve scaling of the same-spin and opposite-spin components of the MP2-like correlation energy, result in RMSDs ranging between 8.7 (XYG3) and 15.0 (B2PLYP) kJ mol^{-1}. The best performing DHDFT methods with RMSDs below the threshold of chemical accuracy are ωB97X-2(LP), ωB97X-2(TQZ), PWPB95, PBEQI-DH, and DSD-PBEB95. It is noteworthy that the parameter-free PBEQI-DH and DSD-PBEB95 result in excellent performance with RMSDs of 1.8 and 1.5 kJ mol^{-1}, respectively.

It is of interest to examine the effect of empirical dispersion corrections on the performance of some of the of DFT functionals for the reaction barrier heights in the CopeBH database. Table 4 gathers the differences in RMSD between the dispersion-corrected and uncorrected DFT functionals. Across all rungs of Jacob's Ladder, inclusion of the D3 correction has a relatively minor effect on the performance of the DFT functionals. For the reaction barrier heights, the D3 correction generally leads to a small increase in the RMSDs by up to 1 kJ mol^{-1}

(Table 4). These minor deteriorations in performance are observed since most DFT functionals tend to underestimate the reaction barrier heights and the dispersion correction tends to systematically reduce the reaction barrier heights.[115] In contrast, for the reaction energies, the D3 correction results in minor reductions in the RMSDs by up to ~2 kJ mol^{-1} (Table 4).

Table 4. Overview of the performance of a representative set of DFT functionals across the rungs of Jacob's Ladder with and without empirical D3 dispersion corrections. The tabulated values are ΔD3 = RMSD(DFT) – RMSD(DFT-D3) (in kJ mol^{-1}).[a]

Type	Method	Barrier heights	Reaction energies
GGA	BLYP	–1.1	1.8
	PBE	–0.5	0.6
	BP86	–1.0	1.6
MGGA	M06L	0.0	–0.1
	TPSS	–0.7	1.1
HGGA	B3LYP	–0.9	1.4
	B3PW91	–0.8	1.7
	PBE0	–0.2	0.8
	APF[b]	–0.5	0.6
	CAM-B3LYP	0.8	1.0
HMGGA	PW6B95	–0.1	0.7
	M05	0.4	0.5
	M05-2X	0.1	0.0
	M06	0.1	0.0
	M06-2X	0.0	0.0
	M06-HF	0.0	0.0
	BMK	–0.7	1.6
DH	B2-PLYP	–0.2	0.8
	DSD-PBEP86[c]	–0.4	0.6

[a]A positive value indicates the dispersion correction improves the performance of the functional, whereas a negative value indicates deterioration in performance. [b]Original dispersion correction used, ΔD3 = RMSD(APF) – RMSD(APF-D). [c]D3BJ dispersion correction used.

Finally, it is of interest to examine the performance of economical composite ab initio procedures for the reaction barrier heights in the CopeBH database. The CBS-QB3 procedure has been previously shown to give poor performance for reaction barrier heights of pericyclic reactions.[29] Namely, relative to CCSD(T)/CBS reference values from W*n*-F12 theories (*n* = 1, 2),[34,35] CBS-QB3 attains an RMSD of 10.0 kJ mol^{-1} over the 26 barrier heights of pericyclic

reactions in the BHPERI database.[29] It is therefore not surprising that CBS-QB3 attains poor performance for the reaction barrier heights in the CopeBH database, with an RMSD of 9.8 kJ mol^{-1}. The economical G4(MP2) and G4(MP2)-6X procedures result in relatively large RMSDs of 6.8 and 5.4 kJ mol^{-1}, respectively. Thus, their use does not seem to be warranted considering their computational cost. The G4 method gives much better performance with an RMSD of 3.0 kJ mol^{-1} and is therefore the only economical composite ab initio procedure that is recommended.

3.3 Performance of DFT and ab initio procedures for the reaction energies in the CopeRE database. All the reactions in the Cope dataset conserve the numbers of each formal bond type and the number of C atoms in each hybridization state on both sides of the reaction (see local minima **1**, **2**, **3**, and **4**, Figure 1). In addition, transformation **1** → **2** conserves the number of C atoms in each hapticity (i.e., primary, secondary, and tertiary) and is therefore hypohomodesmotic.[116] Thus, a priori we would expect DFT methods to exhibit good performance for the reaction energies in the CopeRE dataset.[117,118,119,120] Figure 5 gives an overview of the performance of the DFT functionals for the reaction energies in the CopeRE database. Although the reaction energies are much less challenging for DFT methods than the reaction barrier heights, they still pose a significant challenge for GGA and MGGA functionals. With one exception (MN15-L), none of the GGA and MGGA functionals are able to surpass the threshold of chemical accuracy, with RMSDs ranging between 4.6 (M11-L) and 10.2 (HCTH407) kJ mol^{-1}. The average RMSD over all of the considered GGA and MGGA functionals is 7.5 kJ mol^{-1}. For comparison, for the reaction barrier heights the average RMSD over all of the considered GGA and MGGA functionals is 19.6 kJ mol^{-1}, demonstrating that the reaction barrier heights are much more challenging for these methods.

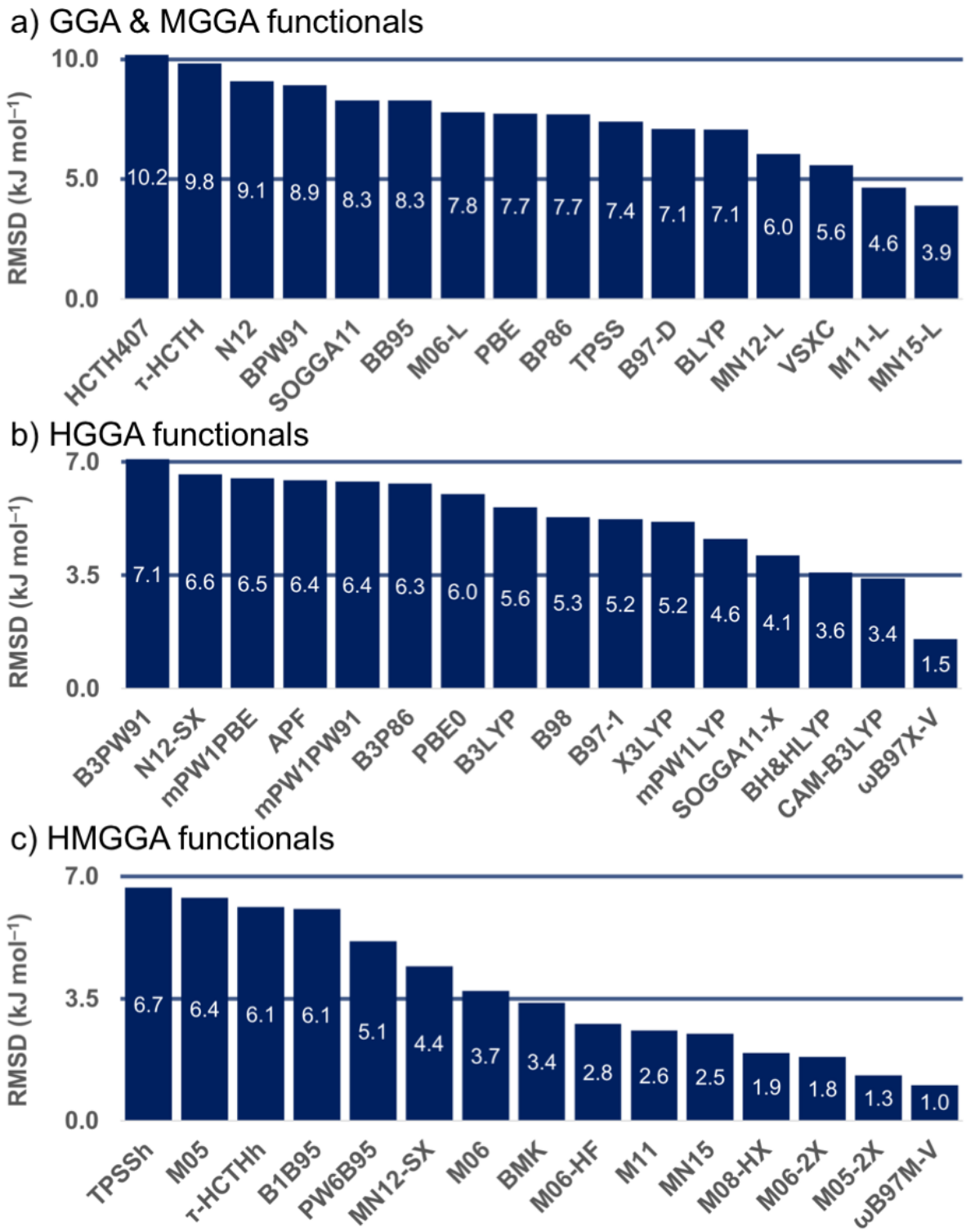

Figure 5. Root-mean-square deviations for (a) GGA and MGGA, (b) HGGA, and (c) HMGGA functionals over the reaction energies in the CopeRE database (in kJ mol^{-1}) (note that GGAs and MGGAs belong to different rungs of Jacob's Ladder but are grouped to save space).

Inclusion of exact exchange in the HGGA functionals results in improvements over the GGA and MGGA functionals. Namely, we obtain RMSDs between 3.6 (BH&HLYP) and 7.1 (B3PW91) kJ mol^{-1}. The range-separated CAM-B3LYP functional shows comparable performance to the global HGGA BH&HLYP with an RMSD of 3.4 kJ mol^{-1}. However, the ωB97X-V range-separated HGGA functional attains a remarkably low RMSD of 1.5 kJ mol^{-1}.

The HMGGA functionals show superior performance for the reaction energies with most functionals attaining RMSDs below the chemical accuracy threshold. In particular, the global hybrids with 52–56% of exact HF exchange show excellent performance with RMSDs of 1.9 (M08-HX), 1.8 (M06-2X), and 1.3 (M05-2X) kJ mol^{-1}. However, the range-separated HMGGA ωB97M-V, which incorporates 15% HF exchange in the short range and 100% HF exchange in the long range, shows exceptionally good performance with an RMSD of merely 1.0 kJ mol^{-1}. For comparison, the global hybrid M06-HF with 100% HF exchange results in an RMSD of 2.8 kJ mol^{-1}.

Figure 6 depicts the RMSDs for the MP2-based and DHDFT methods for the reaction energies in the CopeRE database. All of the considered DHDFT methods show good-to-excellent performance with RMSDs ranging between 4.4 (PBE0-DH) and 0.6 (ωB97X-2(TQZ)) kJ mol^{-1}. It should be noted that the range-separated DHDFT methods ωB97X-2(LP) and ωB97M-V attain sub-kJ-per-mole RMSDs of 0.8 and 0.9 kJ mol^{-1}, respectively. DSD-PBEP86 and XYG3 attain similar performance with an RMSD of 1.2 kJ mol^{-1}.

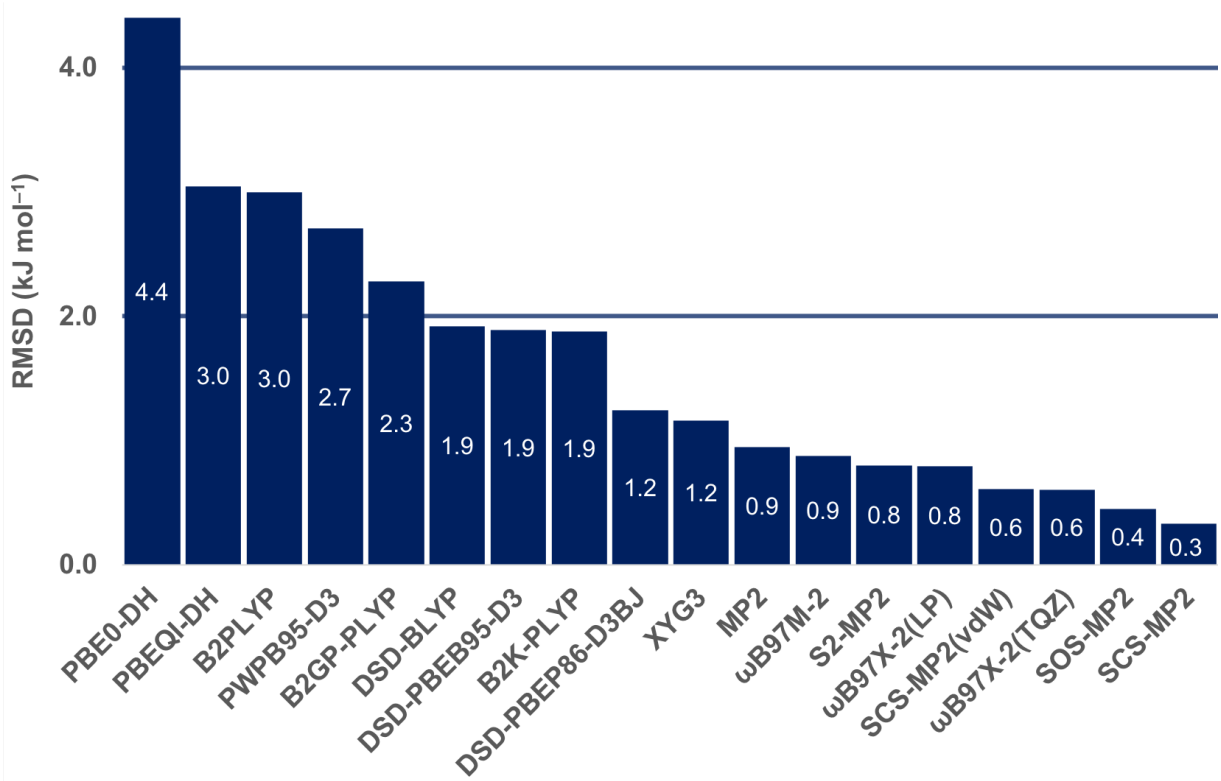

Figure 6. Root-mean-square deviations for DHDFT and standard/composite ab initio methods over the reaction energies in the CopeRE database (in kJ mol^{-1}).

All the MP2-based methods attain sub-kJ-per-mole RMSDs ranging between 0.9 (MP2) and 0.3 (SCS-MP2) kJ mol^{-1}. SOS-MP2 attains similar performance to SCS-MP2 with an RMSD of 0.4 kJ mol^{-1}. Finally, we note that all the approximate composite ab initio methods attain similar performance with RMSDs ranging between 1.0 (G4 and CBS-QB3) and 1.2 (G4(MP2)) kJ mol^{-1}.

3.5 Overall recommendations for both reaction energies and barrier heights. In practical applications, we would like to accurately calculate both reaction energies and barrier heights with high accuracy. Figure S2 of the Supporting Information depicts the average RMSD obtained over the barrier heights in the CopeBH database and the reaction energies in the CopeRE database (the average RMSD is simply the arithmetic average of the RMSDs obtained for the reaction energies and barrier heights). As expected from the results of the previous sections, none of the GGA and

MGGA functionals are able to attain an average RMSD below the threshold of chemical accuracy. The two best performing methods are M06-L and MN15-L with RMSDs of 6.5 and 6.4 kJ mol^{-1}, respectively. It is hard to choose which of these functionals is better suited for the description of both reaction energies and barrier heights in the Cope database. MN15-L attains relatively poor performance for reaction barrier heights (RMSD = 8.9 kJ mol^{-1}) and M06-L attains relatively poor performance for reaction energies (RMSD = 7.8 kJ mol^{-1}).

Overall, the HGGA functionals offer an improvement over the GGA and MGGA methods, with the best performing method PBE0 attaining an RMSD of 5.2 kJ mol^{-1}. We note that PBE0 is the best performing HGGA functional for the reaction barrier heights (RMSD = 4.5 kJ mol^{-1}). Six HMGGA functionals are able to attain RMSD below 5 kJ mol^{-1}, namely 4.9 (B1B95 and MN12-SX), 4.7 (MN15), 4.6 (PW6B95), and 4.2 (BMK and M05-2X) kJ mol^{-1}. Of these, BMK, PW6B95, and MN12-SX offer balanced performance for both reaction energies and barrier heights and are therefore recommend for describing all aspects of the potential energy surface of Cope rearrangements in Bullvalene derivatives.

Figure S3 of the Supporting Information depicts the average RMSDs obtained over the reaction energies and barrier heights for the DHDFT and MP2-based methods. The best performing double-hybrid DFT methods attain RMSDs ≤ 2.5 kJ mol^{-1}, namely (RMSDs are given in parentheses): PWPB95 (2.5), PBEQI-DH (2.4), ωB97X-2(LP) (1.8), DSD-PBEB95 (1.7), and ωB97X-2(TQZ) (1.5 kJ mol^{-1}). All of these functionals attain RMSDs ≤ 3.0 kJ mol^{-1} for both reaction energies and barrier heights and are therefore recommended for investigating similar PESs.

The best performing MP2-based methods are SCS-MP2 and SOS-MP2 with RMSDs of 3.9 and 1.2 kJ mol^{-1}, respectively. SCS-MP2 shows relatively poor performance for reaction barrier heights and is therefore not recommended. However, SOS-MP2 attains RMSDs of merely 0.3 and 1.9 kJ mol^{-1} for reaction energies and barrier heights, respectively. Remarkably, SOS-

MP2 performs better than the composite ab initio methods that are considered in the present work, namely we obtain the following average RMSDs for the composite ab initio methods 5.4 (CBS-QB3), 4.0 (G4(MP2)), 3.3 (G4(MP2)-6X), and 2.0 (G4) kJ mol^{-1}.

4. Conclusions

We introduce a representative benchmark database of 22 reaction barrier heights and 21 reaction energies in substituted bullvalenes ($C_{10}H_9R$, R = NH_3, OH, CH_3, H, F, Cl, SH, and CN) to be known as the Cope22 database. The reference reaction energies and barrier heights are obtained at the CCSD(T)/CBS level by means of the W1-F12 composite method. These high-level benchmark values allow us to assess the performance of DFT functionals across the rungs of Jacob's Ladder as well as MP2-based and computationally economical composite ab initio procedures. With regard to the performance of the DFT procedures we make the following observations:

- Of all the considered DFT methods, only hybrid-meta-GGAs attain good performance for both reaction barrier heights and reaction energies, with the best performing functionals being BMK, PW6B95, and MN12-SX.
- A number of DFT methods attain reasonable performance for reaction barrier heights (RMSDs are given in parentheses), namely the GGA M06-L (5.3); the HGGA PBE0 (4.5); and the HMGGAs BMK (4.9), PW6B95 (4.2), and B1B95 (3.8 kJ mol^{-1}).
- The performance of DFT methods for reaction energies is considerably better than for reaction barrier heights. The best performers from each rung of Jacob's Ladder are (RMSDs given in parentheses): the GGA MN15-L (3.9); the HGGAs BH&HLYP (3.6), CAM-B3LYP (3.4), and ωB97X-V (1.5); and the HMGGAs M08-HX (1.9), M06-2X (1.8), M05-2X (1.3), and ωB97M-V (1.0 kJ mol^{-1}).

With regard to the performance of DHDFT, MP2-based, and composite ab initio procedures, we draw the following conclusions:

- The performance of the MP2-based methods for the reaction barrier heights correlates linearly with the same-spin component (C_{SS}) of the MP2 correlation energy. Namely, we obtain the following RMSDs (method and C_{SS} coefficient are given in parentheses): 25.8 (MP2, 1.00), 21.3 (S2-MP2, 0.75), 15.25 (SCS-MP2(vdW), 0.50), 7.5 (SCS-MP2, 0.33), and 1.9 (SOS-MP2, 0.00) kJ mol^{-1}.
- A number of recently developed DHDFT methods show exceptionally good performance for both reaction energies and barrier heights, with overall average RMSDs of 2.5 (PWPB95), 2.4 (PBEQI-DH), 1.8 (ωB97X-2(LP)), 1.7 (DSD-PBEB95), and 1.5 (ωB97X-2(TQZ)) kJ mol^{-1}. Remarkably, SOS-MP2 outperforms all the DHDFT methods with an average RMSD of merely 1.2 kJ mol^{-1}.
- Of the composite procedures, G4 theory shows the best overall performance with an average RMSD of 2.0 kJ mol^{-1} for both barrier heights and reaction energies.

Supplementary data

Statistical analysis for the performance of DFT, DHDFT, and ab initio procedures for the reaction energies and barrier heights in the Cope database (Table S1); individual errors for the DFT, DHDFT, and ab initio procedures for the reaction energies and barrier heights in the Cope database (Table S2); optimized geometries (Cartesian coordinates) for all the reactants, transition structures, and products in the Cope database (Table S3); W1-F12 reaction barrier heights for **TS**$_{1\text{-}2}$, **TS**$_{2\text{-}3}$, and **TS**$_{3\text{-}4}$ versus the σ_p Hammett constants for the various substituents (Figure S1); average root-mean-square deviations over the reaction energies and barrier heights in the Cope database for DFT functionals (Figure S2); average root-mean-square deviations over the reaction

energies and barrier heights in the Cope database for DHDFT and standard/composite ab initio methods (Figure S3); and full references for quantum chemical software.

Acknowledgments

This research was undertaken with the assistance of resources from the National Computational Infrastructure (NCI), which is supported by the Australian Government. We also acknowledge the system administration support provided by the Faculty of Science at the University of Western Australia to the Linux cluster of the Karton group. The author would also like to thank the reviewers for helpful comments and suggestions.

Funding Information

Australian Research Council (ARC) Future Fellowship (Project No. FT170100373).

References

[1] A. N. Bismillah, B. M. Chapin, B. A. Hussein, P. R. McGonigal, Chem. Sci. 11 (2020) 324.

[2] A. G. Császár, C. Fábri1, J. Sarka, WIREs Comput. Mol. Sci. 10 (2020) e1432.

[3] N. Graulich, WIREs Comput. Mol. Sci. 1 (2011) 172.

[4] M. L. McKee, WIREs Comput. Mol. Sci. 1 (2011) 943.

[5] A. R. Lippert, J. Kaeobamrung, J. W. Bode, J. Am. Chem. Soc. 128 (2006) 14738.

[6] A. R. Lippert, V. L. Keleshian, J. W. Bode, Org. Biomol. Chem. 7 (2009) 1529.

[7] A. R. Lippert, A. Naganawa, V. L. Keleshian, J. W. Bode, J. Am. Chem. Soc. 132 (2010) 15790.

[8] M. He, J. W. Bode, Proc. Natl. Acad. Sci. U.S.A. 108 (2011) 14752.

[9] K. K. Larson, M. He, J. F. Teichert, A. Naganawa, J. W. Bode, Chem. Sci. 3 (2012) 1825.

[10] M. He, J. W. Bode, Org. Biomol. Chem. 11 (2013) 1306.

[11] J. F. Teichert, D. Mazunin, J. W. Bode, J. Am. Chem. Soc. 135 (2013) 11314.

[12] O. Yahiaoui, L. F. Pasteka, B. Judeel, T. Fallon, Angew. Chem. Int. Ed. 57 (2018) 2570.

[13] A. N. Bismillah, J. Sturala, B. M. Chapin, D. S. Yufit, P. Hodgkinson, P. R. McGonigal, Chem. Sci. 9 (2018) 8631.

[14] O. Yahiaoui, L. F. Pasteka, C. J. Blake, C. G. Newton, T. Fallon, Org. Lett. 21 (2019) 9574.

[15] H. D. Patel, T.-H. Tran, C. J. Sumby, L. F. Pasteka, Fallon, T. J. Am. Chem. Soc. 142 (2020) 3680.

[16] M. Khojandi, A. Seif, E. Zahedi, L. R. Domingo, M. Karimkhani. New J. Chem. 44 (2020) 6543.

[17] Y.-Y. Ma, M. Yan, H.-R. Li, Y.-B. Wu , X.-X. Tian, H.-G. Lu, S.-D. Li, Sci. Rep. 9 (2019) 17074.

[18] Y. J. Okamoto, J. Chem. Phys. 150 (2019) 134103.

[19] D. Sharma, M. Ojha, P. Maheshwari, A. Gurjar, R. K. Bansal, Phosphorus Sulfur 190 (2015) 1.

[20] T. Bredtmann, B. Paulus, J. Chem. Theory Comput. 9 (2013) 3026.

[21] P. R. Griffiths, D. E. Pivonka, R. V. Williams, Chem. Eur. J. 17 (2011) 9193.

[22] X. Zhang, D. A. Hrovat, W. T. Borden, Org. Lett. 12 (2010) 2798.

[23] E. C. Brown, R. F. W. Bader, N. H. Werstiuk, J. Phys. Chem. A 113 (2009) 3254.

[24] S. C. Wang, D. J. Tantillo, J. Phys. Chem. A 111 (2007) 7149.

[25] S. Liang, C.-H. Lee, S. I. Kozhushkov, D. S. Yufit, J. A. K. Howard, K. Meindl, S. Rühl, C. Yamamoto, Y. Okamoto, P. R. Schreiner, B. C. Rinderspacher, A. de Meijere, Chem. Eur. J. 11 (2005) 2012.

[26] D. A. Hrovat, E. C. Brown, R. V. Williams, H. Quast, W. T. Borden, J. Org. Chem. 70 (2005) 2627.

[27] H.-S. Wu, H. Jiao, Z.-X. Wang, P. v. R. Schleyer, J. Am. Chem. Soc. 125 (2003) 10524.

[28] E. C. Brown, D. K. Henze, W. T. Borden, J. Am. Chem. Soc. 124 (2002) 14977.

[29] A. Karton, L. Goerigk, J. Comput. Chem. 36 (2015) 622.

[30] S. Grimme, C. Muck-Lichtenfeld, E.-U. Wurthwein, A. W. Ehlers, T. P. M. Goumans, K. Lammertsma, J. Phys. Chem. A 110 (2006) 2583.

[31] D. H. Ess, K. N. Houk, J. Phys. Chem. A 109 (2005) 9542.

[32] V. Guner, K. S. Khuong, A. G. Leach, P. S. Lee, M. D. Bartberger, K. N. Houk, J. Phys. Chem. A 107 (2003) 11445.

[33] T. C. Dinadayalane, R. Vijaya, A. Smitha, G. N. Sastry, J. Phys. Chem. A 106 (2002) 1627.

[34] A. Karton, J. M. L. Martin, J. Chem. Phys. 136 (2012) 124114.

[35] A. Karton, WIREs Comput. Mol. Sci. 6 (2016) 292.

[36] J. P. Perdew, K. Schmidt, AIP Conf. Proc. 577 (2000) 1.

[37] A. Karton, J. Phys. Chem. A 123 (2019) 6720.

[38] A. Karton, N. Sylvetsky, J. M. L. Martin, J. Comput. Chem. 38 (2017) 2063.

[39] A. Karton, P.R. Schreiner, J.M.L. Martin, J. Comput. Chem. 37 (2016) 49.

[40] L.-J. Yu, A. Karton, Chem. Phys. 441 (2014) 166.

[41] S. Grimme, WIREs Comput. Mol. Sci. 1 (2011) 211.

[42] S. Grimme, J. Antony, S. Ehrlich, H. Krieg, J. Chem. Phys. 132 (2010) 154104.

[43] S. Grimme, S. Ehrlich, L. Goerigk, J. Comput. Chem. 32 (2011) 1456.

[44] A. D. Becke, E. R. Johnson, J. Chem. Phys. 123 (2005) 154101.

[45] C. Lee, W. Yang, R. G. Parr, Phys. Rev. B 37 (1988) 785.

[46] A. D. Becke, Phys. Rev. A 38 (1988) 3098.

[47] S. Grimme, J. Comput. Chem. 27 (2006) 1787.

[48] A. D. Boese, N. C. Handy, J. Chem. Phys. 114 (2001) 5497.

[49] J. P. Perdew, K. Burke, M. Ernzerhof, Phys. Rev. Lett. 77 (1996) 3865.

[50] J. P. Perdew, Phys. Rev. B 33 (1986) 8822.

[51] J. P. Perdew, J. A. Chevary, S. H. Vosko, K. A. Jackson, M. R. Pederson, D. J. Singh, C.

Fiolhais, Phys. Rev. B 46 (1992) 6671.

[52] R. Peverati, Y. Zhao, D. G. Truhlar, J. Phys. Chem. Lett. 2 (2011) 1991.

[53] R. Peverati, D. G. Truhlar, J. Chem. Theory Comput. 8 (2012) 2310.

[54] Y. Zhao, D. G. Truhlar, J. Chem. Phys. 125 (2006) 194101.

[55] J. M. Tao, J. P. Perdew, V. N. Staroverov, G. E. Scuseria, Phys. Rev. Lett. 91 (2003) 146401.

[56] A. D. Boese, N. C. Handy, J. Chem. Phys. 116 (2002) 9559.

[57] T. van Voorhis, G. E. Scuseria, J. Chem. Phys. 109 (1998) 400.

[58] A. D. Becke, J. Chem. Phys. 104 (1996) 1040.

[59] R. Peverati, D. G. Truhlar, J. Phys. Chem. Lett. 3 (2012) 117.

[60] R. Peverati, D. G. Truhlar, Phys. Chem. Chem. Phys. 10 (2012) 13171.

[61] H. S. Yu, X. He, S. L. Li, D. G. Truhlar, Chem. Sci. 7 (2016) 5032.

[62] A. D. Becke, J. Chem. Phys. 98 (1993) 1372.

[63] A. D. Becke, J. Chem. Phys. 98 (1993) 5648.

[64] P. J. Stephens, F. J. Devlin, C. F. Chabalowski, M. J. Frisch, J. Phys. Chem. 98 (1994) 11623.

[65] C. Adamo, V. Barone, J. Chem. Phys. 110 (1999) 6158.

[66] F. A. Hamprecht, A. J. Cohen, D. J. Tozer, N. C. Handy, J. Chem. Phys. 109 (1998) 6264.

[67] H. L. Schmider, A. D. Becke, J. Chem. Phys. 108 (1998) 9624.

[68] X. Xu, Q. Zhang, R. P. Muller, W. A. Goddard, J. Chem. Phys. 122 (2005) 014105.

[69] R. Peverati, D. G. Truhlar, J. Chem. Phys. 135 (2011) 191102.

[70] A. Austin, G. Petersson, M. J. Frisch, F. J. Dobek, G. Scalmani, K. Throssell, J. Chem. Theory Comput. 8 (2012) 4989.

[71] C. Adamo, V. Barone, J. Chem. Phys. 108 (1998) 664.

[72] T. Yanai, D. Tew, N. C. Handy, Chem. Phys. Lett. 393 (2004) 51.

[73] N. Mardirossian, M. Head-Gordon, Phys. Chem. Chem. Phys. 16 (2014) 9904.

[74] R. Peverati, D. G. Truhlar, Phys. Chem. Chem. Phys. 14 (2012) 16187.

[75] Y. Zhao, N. E. Schultz, D. G. Truhlar, J. Chem. Phys. 123 (2005) 161103.

[76] Y. Zhao, N. E. Schultz, D. G. Truhlar, J. Chem. Theory Comput. 2 (2006) 364.

[77] Y. Zhao, D. G. Truhlar, Theor. Chem. Acc. 120 (2008) 215.

[78] Y. Zhao, D. G. Truhlar, J. Chem. Theory Comput. 4 (2008) 1849.

[79] A. D. Boese, J. M. L. Martin, J. Chem. Phys. 121 (2004) 3405.

[80] V. N. Staroverov, G. E. Scuseria, J. Tao, J. P. Perdew, J. Chem. Phys. 119 (2003) 12129.

[81] Y. Zhao, D. G. Truhlar, J. Phys. Chem. A 109 (2005) 5656.

[82] R. Peverati, D. G. Truhlar, J. Phys. Chem. Lett. 2 (2011) 2810.

[83] N. Mardirossian, M. Head-Gordon, J. Chem. Phys. 144 (2016) 214110.

[84] S. Grimme, J. Chem. Phys. 124 (2006) 034108.

[85] A. Karton, A. Tarnopolsky, J.–F. Lamere, G. C. Schatz, J. M. L. Martin, J. Phys. Chem. A 112 (2008) 12868.

[86] A. Tarnopolsky, A. Karton, R. Sertchook, D. Vuzman, J. M. L. Martin, J. Phys. Chem. A 112 (2008) 3.

[87] S. Kozuch, D. Gruzman, J. M. L. Martin, J. Phys. Chem. C 114 (2010) 20801.

[88] S. Kozuch, J. M. L. Martin, J. Comput. Chem. 34 (2013) 2327.

[89] S. Kozuch, J. M. L. Martin, Phys. Chem. Chem. Phys. 13 (2011) 20104.

[90] É. Brémond, C. Adamo, J. Chem. Phys. 135 (2011) 024106.

[91] Y. Zhang, X. Xu, W. A. Goddard III, Proc. Natl. Acad. Sci. U.S.A. 106 (2009) 4963.

[92] L. Goerigk, S. Grimme, J. Chem. Theory Comput. 7 (2011) 291.

[93] É. Brémond, J. C. Sancho-García, Á. J. Pérez-Jiménez, C. Adamo, J. Chem. Phys. 141 (2014) 031101.

[94] J.-D. Chai, M. Head-Gordon, J. Chem. Phys. 131 (2009) 174105.

[95] N. Mardirossian, M. Head-Gordon, J. Chem. Phys. 148 (2018) 241736.

[96] R. F. Fink, J. Chem. Phys. 133 (2010) 174113.

[97] S. Grimme, J. Chem. Phys. 118 (2003) 9095.

[98] R. A. King, Mol. Phys. 107 (2009) 789.

[99] Y. Jung, R. C. Lochan, A. D. Dutoi, M. Head-Gordon, J. Chem. Phys. 121 (2004) 9793.

[100] L. A. Curtiss, P. C. Redfern, K. Raghavachari, J. Chem. Phys. 126 (2007) 084108.

[101] L. A. Curtiss, P. C. Redfern, K. Raghavachari, J. Chem. Phys. 127 (2007) 124105.

[102] B. Chan, J. Deng, L. Radom, J. Chem. Theory Comput. 7 (2011) 112.

[103] J. A. Montgomery Jr, M. J. Frisch, J. W. Ochterski, G. A. Petersson, J. Chem. Phys. 110 (1999) 2822.

[104] A. Karton, J. M. L. Martin, J. Chem. Phys. 135 (2011) 144119.

[105] F. Weigend, R. Ahlrichs, Phys. Chem. Chem. Phys. 7 (2005) 3297.

[106] H.-J. Werner, P. J. Knowles, G. Knizia, F. R. Manby, M. Schutz, P. Celani, T. Korona, R. Lindh, A. Mitrushenkov, G. Rauhut, et al. MOLPRO (version 2012.1) is a package of ab initio programs. Available at: http://www.molpro.net.

[107] H.-J. Werner, P. J. Knowles, G. Knizia, F. R. Manby, M. Schutz, WIREs Comput. Mol. Sci. 2 (2012) 242.

[108] M. J. Frisch, G. W. Trucks, H. B. Schlegel, G. E. Scuseria, M. A. Robb, J. R. Cheeseman, G. Scalmani, V. Barone, G. A. Petersson, H. Nakatsuji, et al. Gaussian 16, Revision A.03; Gaussian, Inc., Wallingford, CT, 2016.

[109] Y. H. Shao, Z. T. Gan, E. Epifanovsky, A. T. B. Gilbert, M. Wormit, J. Kussmann, A. W. Lange, A. Behn, J. Deng, X. T. Feng, et al. Mol. Phys. 113 (2015) 184.

[110] R. C. Geary, Biometrika 27 (1935) 310.

[111] R. C. Geary, Biometrika 28 (1936) 295.

[112] A. Karton, R. J. O'Reilly, L. Radom, J. Phys. Chem. A 116 (2012) 4211.

[113] J. Baker, J. Andzelm, M. Muir, P. R. Taylor, Chem. Phys. Lett. 232 (1995) 53.

[114] J. L. Durant, Chem. Phys. Lett. 256 (1996) 595.

[115] C. D. Smith, A. Karton, J. Comput. Chem. 41 (2020) 328.

[116] S. E. Wheeler, K. N. Houk, P. v. R. Schleyer, W. D. Allen, J. Am. Chem. Soc. 131 (2009) 2547.

[117] M. D. Wodrich, C. Corminboeuf, S. E. Wheeler, J. Phys. Chem. A 116 (2012) 3436.

[118] S. E. Wheeler, WIREs Comput. Mol. Sci. 2 (2012) 204.

[119] A. Karton, D. Gruzman, J. M. L. Martin, J. Phys. Chem. A 113 (2009) 8434.

[120] R. O. Ramabhadran, K. Raghavachari, J. Chem. Theory Comput. 7 (2011) 2094.

Graphical TOC